Chapter Six:

NLRX1 localizes to mitochondrial RNA granules and regulates mitochondrial RNA processing and metabolic adaptation

Recent reports from our lab and others demonstrated that mitochondrial immune signaling proteins are widely expressed in non-immune cells and their levels are altered during tumor progression (Bhatelia et al., 2014a; Singh et al., 2015). Similarly, we observed in the current study as discussed in Chapter One that NLRX1 modulates TNF-α-regulated mitochondrial function and cell death. NLRX1 is an unique mitochondria-localized NLR protein and its role in regulating mitochondrial metabolism and cell survival during inflammatory response and tissue injury is emerging (Singh et al., 2015; Stokman et al., 2017). However, its sub-mitochondrial localization and molecular mechanism of regulating mitochondrial function is not well understood. Here, we systematically characterized the sub-mitochondrial localization of NLRX1 and its role in regulating the supramolecular organization of OxPhos system and the energy-generating function of mitochondria.

6.1 NLRX1 localizes to the mitochondrial matrix

NLRX1 is a ubiquitously expressed, highly conserved multi-domain protein of 975 amino acids (Tattoli et al., 2008) having a N-terminal mitochondria-targeting sequence (MTS), a central nucleotide-binding and oligomerization domain (NOD) and putative ligand-binding and regulatory leucine-rich repeat (LRR) domain at the C-terminal end (Arnoult et al., 2009). The analysis of protein expression showed high levels of NLRX1 in some cancer cell lines, such as MDA-MB-231, SHSY-5Y, HepG2 and HeLa, whereas its levels were low in HEK293 and MCF-7 and absent in T47D cells (Fig. 6.1A and B).

We analyzed the subcellular localization of different domain deleted version of NLRX1 through ectopic expression of full length (FL) NLRX1 (1-975 aa), NLRX1 ΔN-ter (160-975 aa) and LRR (564-975 aa) in HEK293 cells by immunoblotting (Fig. 6.1C). We observed a 110 kDa band of full length NLRX1 detected predominantly in mitochondrial fraction although low level of NLRX1 was also detected in the cytosol. N-terminal deletion (NLRX1 ΔN-ter) and only LRR domain (NLRX1-LRR) variants of NLRX1 were found exclusively in the cytosolic fraction confirming that the N-terminal domain of NLRX1 is essential for its translocation to mitochondria.

To examine the localization of NLRX1 to various compartments of mitochondria, mitoplasts from HeLa cells were prepared by selective disruption of the mitochondrial outer

membrane with digitonin and analyzed by western blotting. A band of 110 kDa corresponding to NLRX1 was detect ed in mitoplast fraction. Similarly, 45 kDa and 25 kDa bands corresponding to Citrate Synthase (CS, mitochondrial matrix protein), and ATPase6 (inner mitochondrial membrane protein), respectively, were detected in mitoplast fraction (Fig. 6.1D). As expected, the outer membrane protein Tom20, the intermembrane protein AIF and the cytosolic protein RPS9 were absent in mitoplasts fraction. Similar to CS and ATPase6 proteins, NLRX1 remained intact when mitoplast was digested in the Proteinase K protection assay but acquired a full sensitivity to Proteinase K after permeabilization with Triton X-100 (Fig. 6.1E). In contrast, Tom20 was sensitive to digestion even in the absence of Triton X-100. The alkaline carbonate extraction of isolated mitoplast demonstrated that NLRX1 is not an intrinsic inner membrane protein but was extractable alongside soluble protein CS (Fig. 6.1F). Altogether, these results suggested that NLRX1 is a soluble mitochondrial matrix protein.

We also monitored the submitochondrial of NLRX1 by live-cell confocal microscopy. NLRX1-GFP was ectopically expressed in MCF-7 cells and mitochondria was visualized by staining cells with TMRM, a cell-permeant cationic fluorescent dye which accumulates in mitochondria. We observed a partial but distinct overlap of the GFP fluorescence with the TMRM positive mitochondrial network (up to 60 %) (Fig. 6.1G). The line-scan profile analysis revealed a near-complete overlay of NLRX1-GFP and TMRM intensity, suggesting that NLRX1 exclusively localizes to mitochondria. A recent study using diffraction-unlimited stimulated emission depletion (STED) imaging revealed that TMRM preferentially accumulates at the inner mitochondrial membrane, rather than in the matrix (Ishigaki et al., 2016). Therefore, we transiently co-expressed a mitochondrial matrix-targeted red fluorescent protein (mtRFP) and NLRX1-GFP in HeLa cells and observed a punctate distribution of NLRX1 (shown in grayscale) colocalizing with mitochondria (Fig. 6.1H). The colocalization analysis revealed more than 70 % overlap of distinct green puncta of NLRX1-GFP with positive red signals from mtRFP. These results strongly suggested a predominant localization of NLRX1 to mitochondrial matrix in cells of different origin.

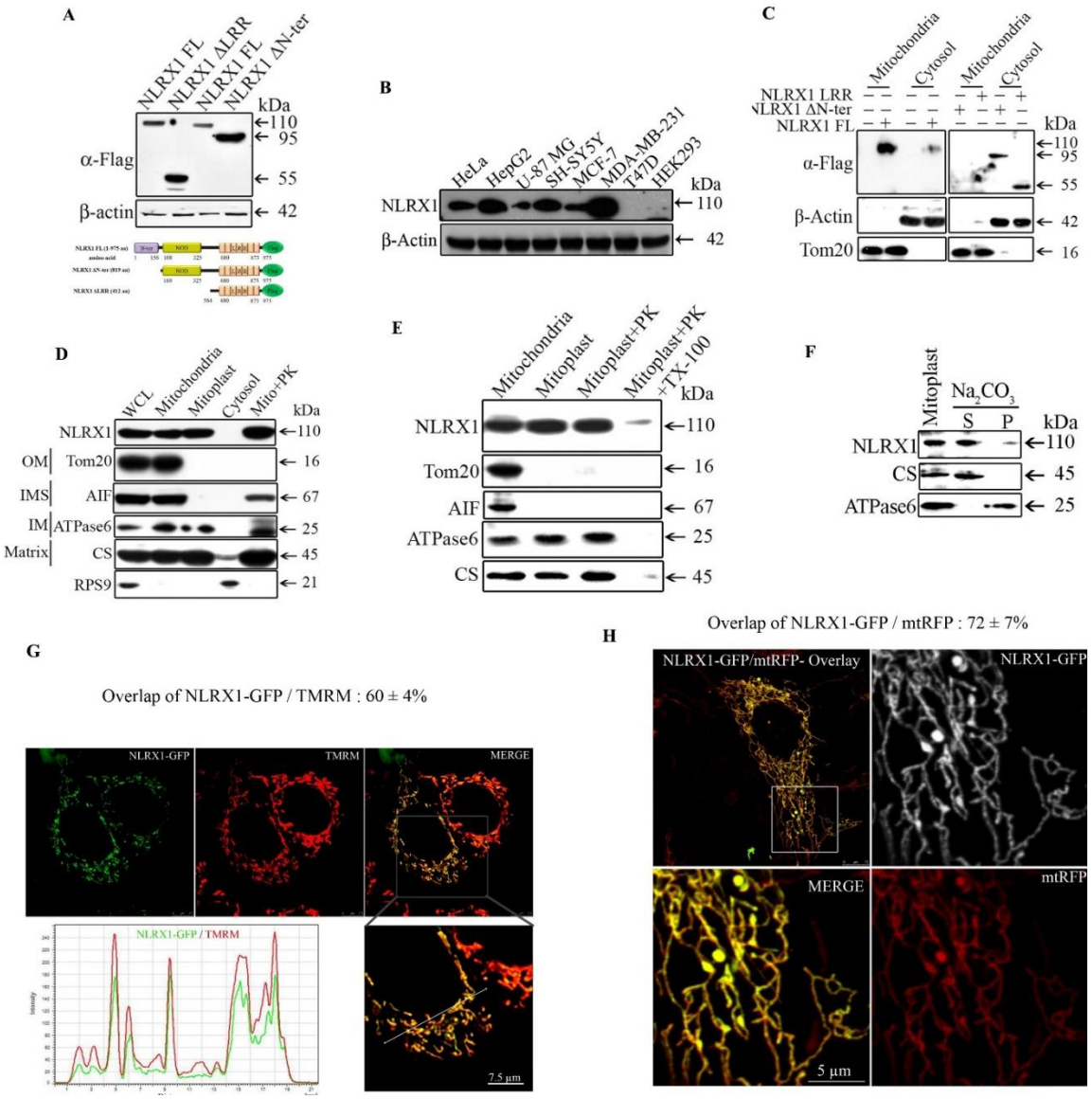

Figure 6.1: NLRX1 resides in the mitochondrial matrix. (A) *Expression profile of the NLRX1 constructs determined by western blotting using anti-Flag antibody in HEK293 cells. Schematic representation of the deletion constructs of NLRX1 used in the study.* ***(B)*** *Endogenous level of NLRX1 in different cell lines was detected by western blotting using anti-NLRX1 antibody.* ***(C)*** *HEK293 cells were transfected with indicated constructs, heavy membrane (mitochondria) and light membrane (cytosol) fractions were isolated and analyzed by western blotting using indicated antibodies.****(D)*** *and* ***(E)*** *Mitochondrial and cytosolic fractions were isolated from HeLa cells, mitoplasts were digested with Proteinase K in the absence or presence of Triton X-100 as described in Materials and methods and analyzed by western blotting using indicated antibodies.****(F)*** *Mitoplasts pellet was subjected to alkaline extraction and ultra-centrifugation to allow the separation of soluble matrix protein (S) and integral protein of inner membrane (P) and analyzed by western blotting.****(G)*** *MCF-7 cells were transfected with NLRX1-GFP and mitochondria were stained with TMRM and analyzed*

by confocal microscopy. Scale bar, 7.5 µm (Merge and inset image). Pixel intensity distribution profile depicts colocalization of NLRX1 and TMRM fluorescence. ***(H)*** *HeLa cells were co-transfected with mtRFP and NLRX1-GFP and observed under confocal microscope. Scale bar, 10 µm (Merge image) and 5 µm (inset image). Pearson's correlation coefficients for NLRX1-GFP/TMRM and NLRX1-GFP/ mtRFP are represented as percent mean ± SD value from n ≥ 5 NLRX1-GFP positive cells.*

6.2 NLRX1 interacts with FASTKD5 and colocalizes with mitochondrial RNA granules

The functional importance of mitochondrial matrix-localization of NLRX1 is not understood. A high-throughput proteomic study of human innate immunity network predicted the interaction of NLRX1 with FASTKD5 (Li et al., 2011) hence this interaction was further analyzed by co-immunoprecipitation experiments. The pulldown of NLRX1 corresponding to a band of 110 kDa was detected in immunoprecipitation of endogenous FASTKD5 suggesting their interaction in normal cellular condition (Fig. 6.2A). This interaction was specific as another mitochondrial RNA granule protein LRPPRC (leucine-rich pentatricopeptide repeat containing protein) and translation elongation factor, EF-Tu were not detected in the FASTKD5 immunoprecipitates. We also immunoprecipitated NLRX1 from cells co-transfected with NLRX1 and FASTKD5 and detected a band of 87 kDa corresponding to FASTKD5, as an NLRX1 interacting protein both in HEK293 and MCF-7 cells (Fig. 6.2B).

We further monitored the colocalization of NLRX1-GFP and FASTKD5-RFP in HEK293-mtCFP stable cells by confocal microscopy. Analysis of line-scan profile showed almost complete overlap of fluorescence intensity of NLRX1-GFP and FASTKD5-RFP. The triple-color overlay image showed distinct colocalization (up to 80%) of NLRX1-GFP and FASTKD5-RFP signals (Fig. 6.2C). Both NLRX1-GFP and FASTKD5-RFP proteins formed distinct puncta across the tubular distribution of mtCFP positive mitochondria. To characterize the size and distribution of distinct punctate structures formed by NLRX1 and FASTKD5, we performed dual-color 3D-SIM (three-dimensional structured illumination microscopy) super-resolution imaging of MCF-7 cells co-expressing NLRX1-GFP and FASTKD5-RFP (Fig. 6.2D). Both NLRX1 and FASTKD5 were concentrated in discrete foci and their fluorescence intensity overlapped

by 60%. The colocalization of NLRX1 and FASTKD5 was also analyzed in XZ-plane with size of focal structures varying between 50-100 nm (Fig. 6.2D'). The fluorescence intensity profile showed complete overlap of NLRX1-GFP and FASTKD5-RFP with size of colocalizing foci ranging from 30-100 nm in the XY-plane.

The recent reports demonstrated that FASTKD5 is a bonafide component of mitochondrial RNA granules (MRGs) (Jourdain et al., 2017). The interaction and colocalization of FASTKD5 and NLRX1 indicated their recruitment to the site of MRGs in mitochondrial matrix. To test this hypothesis, we performed indirect immunofluorescence staining using antibody against BrU-labelled nascent mt-mRNAs and analyzed the degree of colocalization with NLRX1-GFP and FASTKD5-RFP proteins. We observed distinct MRGs foci along the tubular mitochondrial network, where NLRX1-GFP and FASTKD5-RFP colocalized with BrU puncta (65.2 % and 62.7 % respectively) (Fig. 6.2E, F and F'). The line-scan profile analysis revealed a punctate distribution of NLRX1 (in gray scale) overlapping with BrU-labelled nascent mt-mRNAs. The cross-correlation analysis of composite images revealed a gaussian distribution profile with Pearson's coefficient of $P_{NLRX1\text{-}BrU}$= 0.961 and $P_{FASTKD5\text{-}BrU}$ = 0.935 at the ΔX values approaching zero suggesting that both NLRX1 and FASTKD5 co-localize to MRGs (Fig. 6.2G and H). The co-localization of NLRX1 and FASTKD5 within the MRGs suggested their possible role in regulating the post-transcriptional processing of mt-mRNAs.

We further analyzed the colocalization of NLRX1-GFP and FASTKD5-RFP proteins with BrU-labelled MRGs in HEK293-mtCFP stable cells (Fig. 6.2I). As observed above, both FASTKD5-RFP and NLRX1-GFP formed punctate substructures within mitochondria (shown in grayscale). More than fifty percent of FASTKD5-RFP and NLRX1-GFP punctate structures co-localized with BrU-labeled MRGs suggesting that both FASTKD5 and NLRX1 associated with nascent mRNAs in mitochondria (Fig. 6.2J). The analysis of line-scan profiles revealed a major overlap of NLRXI-GFP and FASTKD5-RFP fluorescence with the BrU signal across CFP-labeled mitochondria (Fig. 6.2K). To examine the effect of NLRX1 on RNA granule stability, we knocked down NLRX1 in HeLa cells and visualized for the BrU positive foci (Fig. 6.2K, L and M). The relative number and distribution

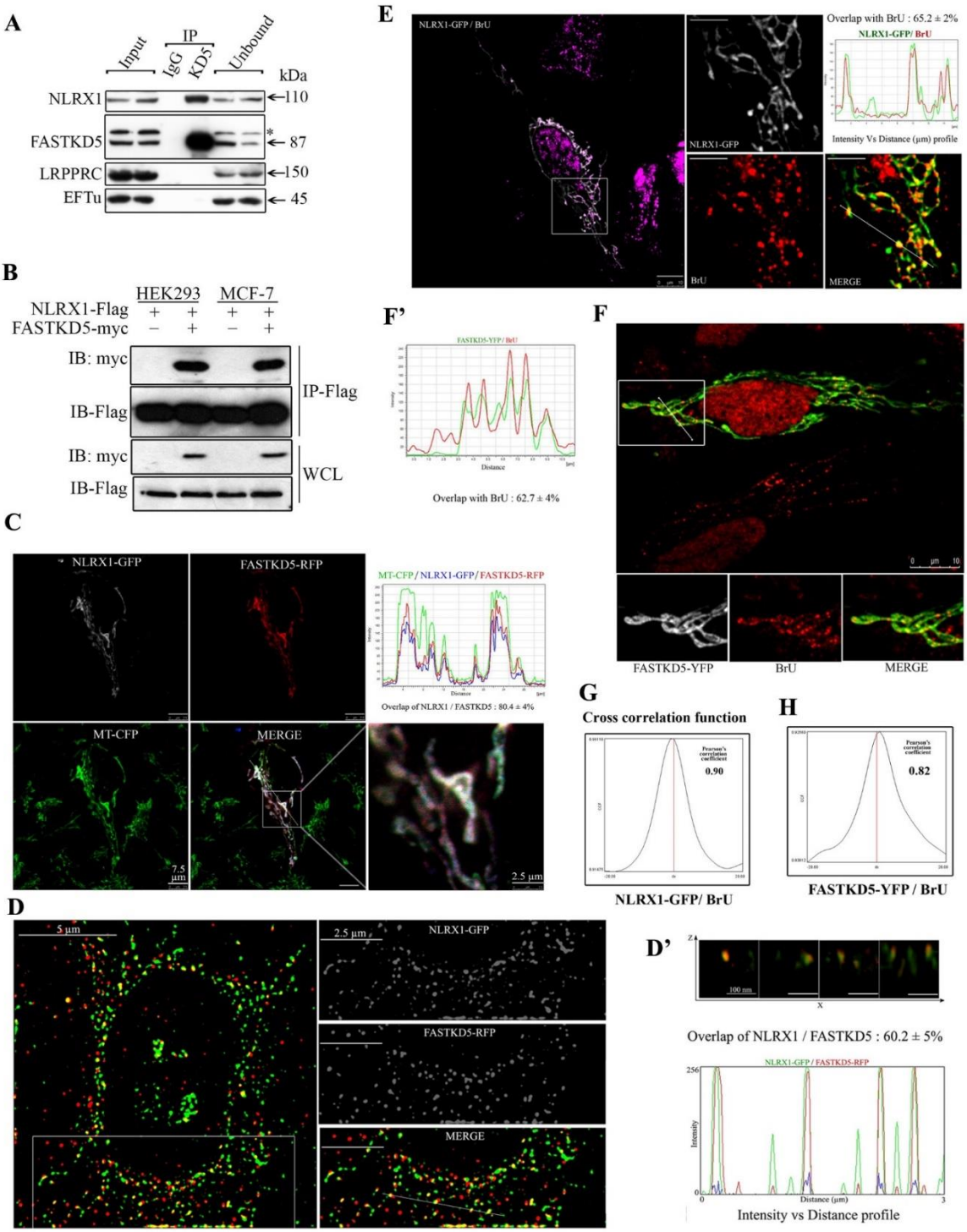

Figure 6.2: NLRX1 interacts with FASTKD5 and resides in the mitochondrial RNA granules. (A) *Co-immunoprecipitation of FASTKD5 was performed using control IgG or anti-FASTKD5 antibody and interacting proteins were analyzed by western blotting using indicated antibodies. Asterisk (*) indicate a non-specific band.* ***(B)*** *FASTKD5 co-immunoprecipitate with NLRX1 in a reciprocal IP. HEK293 cells were co-*

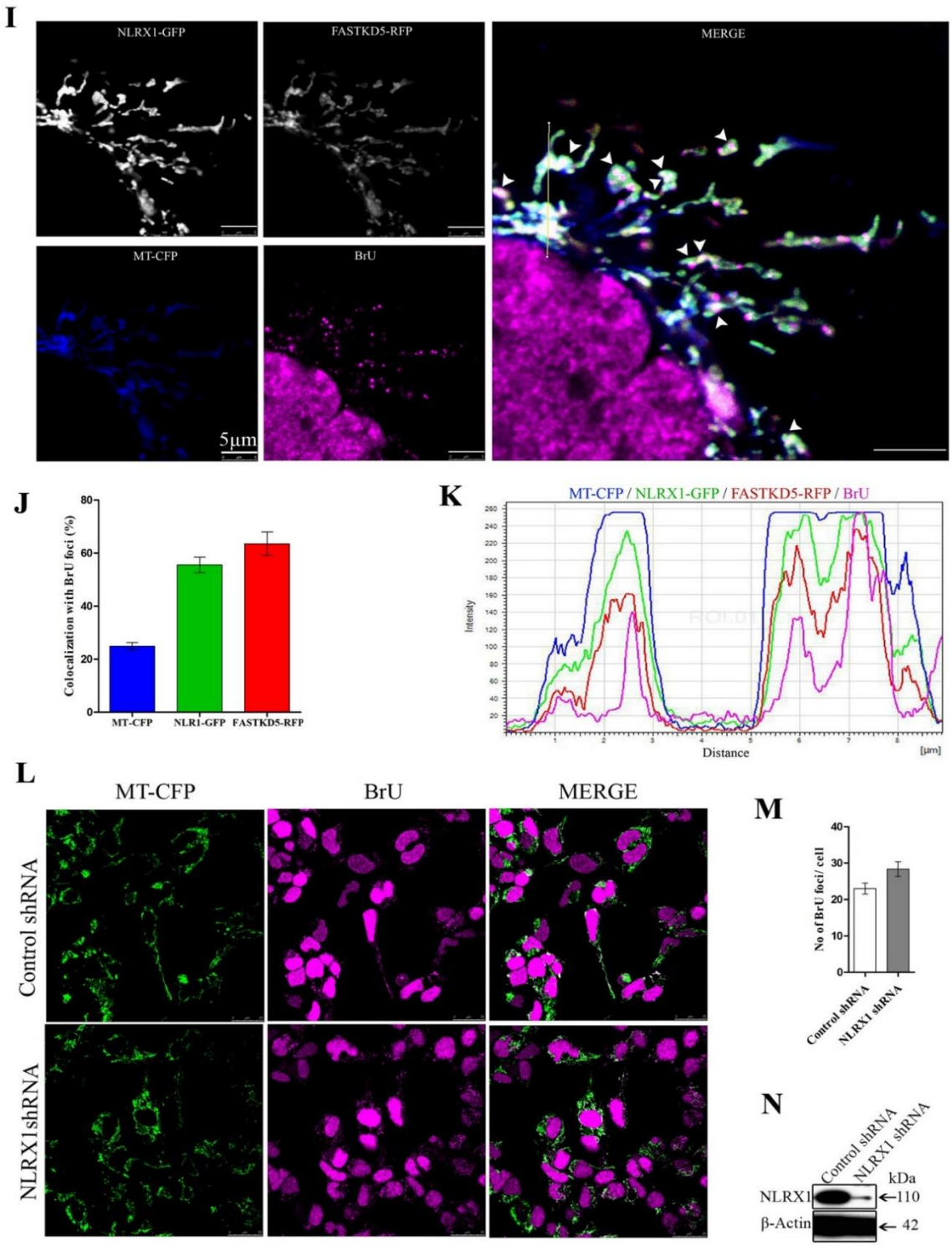

*transfected with NLRX1- Flag and FASTKD5-myc and co-IP was performed using anti-Flag antibody and analyzed by western blotting using indicated antibodies. WCL represents expression of proteins in whole-cell lysates.**(C)** mtCFP-HEK293 stable cells were co-transfected with NLRX1-GFP and FASTKD5-RFP and visualized by confocal microscope. Intensity distribution profile shows colocalization of NLRX1 and*

FASTKD5 with mitochondria. Scale bar, 7.5 µm (Merge image) and 2.5 µm (inset image). Quantification of NLRX1 overlap with FASTKD5 from ≥3cells is shown as mean ± SD alongside intensity profile. ***(D)*** *and* ***(D')*** *Dual-color 3D-SIM image analysis of MCF-7 cells co-transfected with NLRX1-GFP and FASTKD5-RFP. Enlarged view of boxed region is shown on right with Pearson's correlation coefficients for NLRX1-GFP/FASTKD5-RFP represented as percent mean ± SD value. Line scan shows the pixel intensity profile of each fluorescence signal along a line of 3 µm. Colocalization of NLRX1-GFP/FASTKD5-RFP foci along the line scan is shown in a 200 nm thick XZ plane. Scale bar, 5 µm (Merge image) and 2.5 µm (inset image).* ***(E)***, ***(F)*** *and* ***(F')*** *HeLa cells were transfected with either NLRX1-GFP or FASTKD5-RFP and immunofluorescence was performed using anti-BrdU antibody. Quantification of NLRX1/FASTKD5 overlap with BrU from ≥4 cells is shown as mean ± SD. Intensity distribution profile shows the overlap of NLRX1-GFP/FASTKD5-RFP signal with BrU. Scale bar, 10 µm (Merge image) and 2.5 µm (inset image).****(G)*** *and* ***(H)*** *Cross-correlation analysis of BrU foci with NLRX1-GFP or FASTKD5-YFP signal, the high Pearson's coefficient at dx values close to zero indicates that NLRX1-GFP or FASTKD5-YFP signal colocalizes with BrU foci. Pearson's correlation coefficient values for NLRX1-GFP and FASTKD5-YFP with BrU are shown on the right.* ***(I)*** *mtCFP-HEK293 stable cells were co-transfected with NLRX1-GFP and FASTKD5-RFP and immunofluorescence was performed using anti-BrdU antibody and observed under confocal microscope. Scale bar, 5 µm.* ***(J)*** *Quantification of BrU foci with mtCFP, NLRX1 and FASTKD5 signal (arrowheads) for inset image of (I). Data are shown as mean ± SEM (N ≥ 5 cells with ≥15 foci per cell; in total 75 foci were analyzed).* ***(K)*** *Intensity profiles demonstrate the spatial overlap of NLRX1 and FASTKD5 with BrU signal along the line scan.* ***(L)*** *HeLa cells were transfected with control shRNA and NLRX1 shRNA and indirect immunofluorescence was performed using anti-BrdU antibody and observed under confocal microscope.* ***(M)*** *No. of BrU foci per cell were counted and plotted from minimum 50 cells. Data is represented as mean ± SEM, (n=3) Scale bar, 20 µm.* ***(N)*** *Knockdown of NLRX1 in (L) was confirmed by western blotting.*

of the BrU positive foci remained unaltered in the NLRX1 KD HeLa cells indicating that NLRX1 is not essential for the formation of MRGs. These results demonstrated that NLRX1 is a novel protein component of the mitochondrial RNA granules where it interacts with FASTKD5 and colocalizes with nascent mitochondrial RNAs.

6.3 NLRX1 regulates the post-transcriptional processing of non-canonical precursor transcripts in mitochondria

The interaction of NLRX1 with FASTKD5 and its localization to MRGs suggested its potential involvement in the post-transcriptional processing of mitochondrial precursor transcripts. Therefore, we analyzed the steady-state levels of mature mt-RNAs in NLRX1-

KD HeLa cells by qPCR. The knockdown of NLRX1 upregulated the levels of COX I, COX II, ATP8, ATP6, COX III, ND5 and cyt b mRNAs which are products of non-canonical mt-mRNAs processing (Fig. 6.3A and A'). Conversely, ectopic expression of NLRX1 in HEK293 cells decreased the levels of 16S rRNA and all mature mt-mRNAs except ND2, ND4, ND4L, ND3 and ND6 genes. As expected, the over-expression of NLRX1 ΔN-ter showed no significant decrease in the steady-state levels of mt-mRNAs and 16SrRNA as compared to vector control (Fig. 6.3B and B'). We further quantified the alteration in mtDNA copy number in NLRX1-transfected cells (Fig. 3C). The ectopic expression of NLRX1 did not showed significant changes in levels of mtDNA content, thus, ruling out the possibility of mtDNA depletion as a mechanism for the observed decrease in steady-state levels of mitochondrial transcripts. The results suggested that NLRX1 may selectively regulate the steady-state levels of a subset of mt-mRNAs.

We hypothesized that NLRX1 may regulate the post-transcriptional processing of mitochondrial precursor transcripts which is downstream of mtDNA replication. The precursor mRNA regions corresponding to pairs of adjacent genes were selectively amplified by PCR as described previously (Sripada et al., 2017). The ectopic expression of NLRX1 led to an increased accumulation of 1523-bp and 1015-bp PCR products corresponding to the processing intermediates of ATP8+COX III and ND5+cyt b non-junctional heavy strand transcripts (Fig. 6.3D and D'). The levels of the remaining pairs of adjacent genes, such as 16S rRNA-ND1, ND1-ND2 and ND2-COX I, remain unchanged. The knockdown of FASTKD5 in HEK293 cells showed a similar processing defect which resulted in accumulation of ATP8/6+COX III and ND5+cyt b heavy-strand transcripts (Fig. 6.3E and E') as previously reported (Antonicka and Shoubridge, 2015). We confirmed these observations by quantifying the levels of processing intermediates of fused transcripts in a non-strand specific manner using a qPCR approach in T47D cells (Fig. 6.3F and F'). We detected the accumulation of unprocessed form of ATP8/6+COX III and ND5 transcript by two and three-fold higher respectively in NLRX1 transfected cells. However, the COX I + COX II transcript punctuated by $tRNA^{Ser}$ and $tRNA^{Asp}$ as well as ND6 and cyt b transcript punctuated by $tRNA^{Glu.}$ was processed normally. Altogether, these data demonstrated that NLRX1 regulates the post-transcriptional processing of non-canonical ATP8/6+COX III and ND5+cyt b heavy strand transcripts.

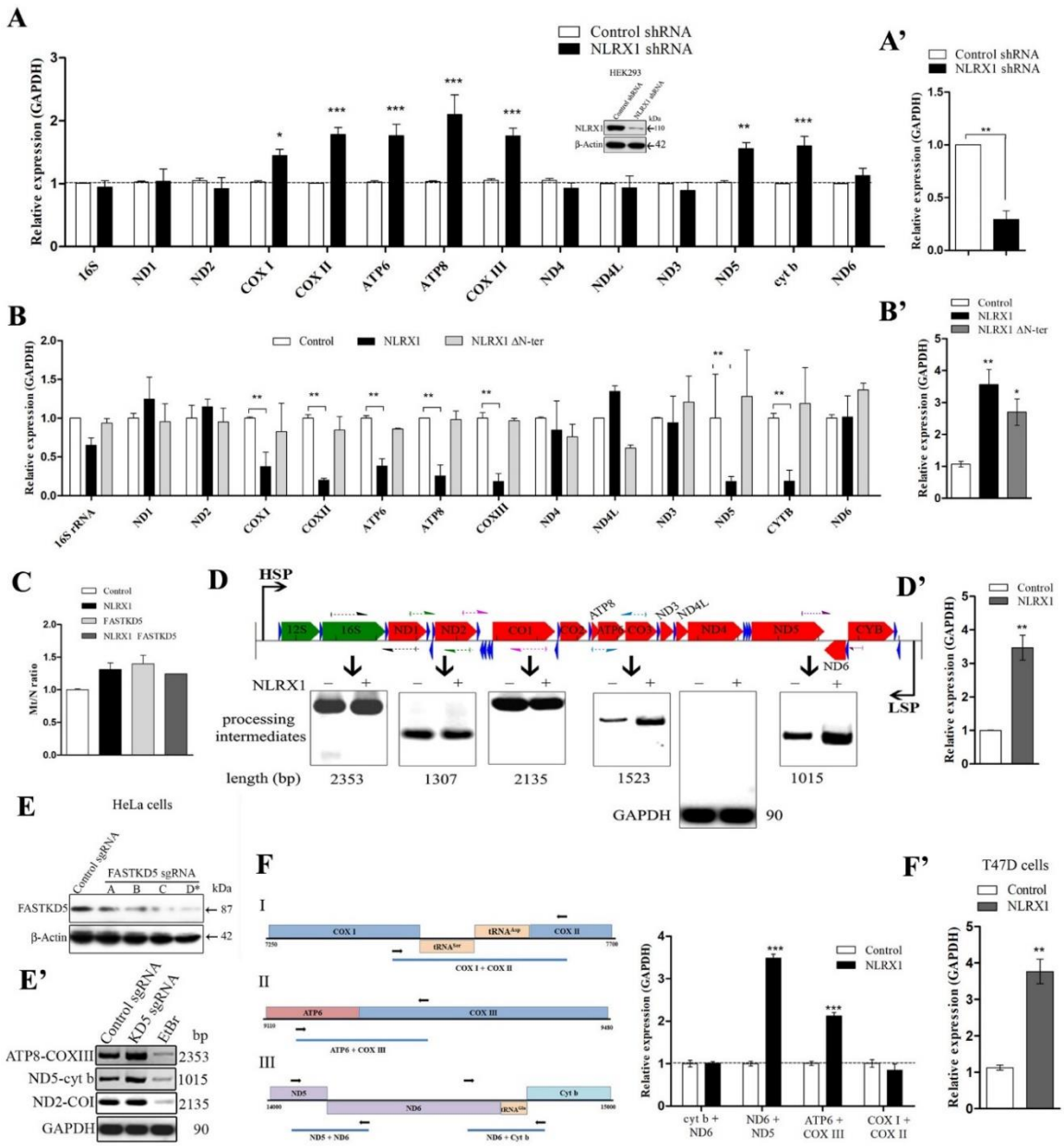

Figure 6.3: NLRX1 affects the post-transcriptional processing of mitochondrial transcript regulated by FASTKD5. (A) and (A') *HeLa cells were transfected with Control shRNA and NLRX1 shRNA and levels of mature mitochondrial genome-encoded transcripts were determined by qPCR. Confirmation of knockdown of NLRX1 in HeLa cells by qPCR and immunoblotting.* ***(B)*** *and* ***(B')*** *HEK293 cells were transfected with control vector, full length NLRX1 and N-terminal deletion mutant of NLRX1 (NLRX1 ΔN-ter) and levels of mature mitochondrial genome-encoded transcripts were determined by qPCR. Confirmation of expression of NLRX1 and NLRX1 ΔN-ter relative to nuclear control (GAPDH) was done by qPCR.* ***(C)*** *HEK293 cells were transfected with indicated constructs and mtDNA levels were quantified by qPCR as described in Materials and method section.* ***(D)*** *and* ***(D')*** *Linear representation of the mitochondrial genome. Green, rRNA; red, mRNA; blue, tRNA. HSP, heavy-strand promoter. LSP, light-strand promoter. Color-coded and half-headed*

arrow pair represents the PCR amplifying RNA regions. HEK293 cells were transfected with NLRX1 and the levels of processing intermediates indicated on linear mitochondrial genome map were analyzed as described in materials and methods. GAPDH was included as nuclear control. Confirmation of NLRX1 expression relative to GAPDH was quantified by qPCR. ***(E)*** *and* ***(E')*** *CRISPR/Cas9-mediated knockout cell line of FASTKD5 was generated in HeLa cells and clone D was further used for analysis of RNA processing by PCR as described in Materials and methods. Transcriptional inhibition by EtBr (1µg/ml for 6 h) was used as positive control.* ***(F)*** *and* ***(F')*** *PCR- quantification of junction-less transcripts: I- COX I + COX II indicated primer sets generating amplification product only when* $tRNA^{Ser}$ *and* $tRNA^{Asp}$ *are unprocessed. II-ATP6 + COX III indicate primer pair for the fragment when the adjacent COXIII and ATPase6 transcripts are unprocessed. III-ND5 + ND6 and ND6 + cyt b indicate primer sets generating product when their respective antisense strands are unprocessed. T47D cells were transfected with vector control and quantitation of expression using these primer pairs (Table) relative to GAPDH was performed. Relative expression of NLRX1 was determined by qPCR. Data are representative of three independent experiments, and the results are expressed as mean ± SD. Asterisk (*) denotes significant differences with* $p < 0.05$.

6.4 NLRX1 regulates the binding of mitochondrial RNA transcripts to FASTKD5

To further understand the apparent decrease in the steady state levels of mature mitochondrial RNAs regulated by NLRX1, we ectopically expressed FASTKD5 and NLRX1 either alone or in combination in HEK293 cells and analyzed the enrichment of target transcripts bound by FASTKD5 or NLRX1 using RNA-IP. The analysis of FASTKD5 immunoprecipitate revealed more than twenty-fold enrichment of almost all long-lived COX I, COX II, COX III mRNAs and 16S rRNA except for ATP8 and ATP6 (Fig. 6.4A and A'). We also observed a low but significant enrichment of short-lived ND5 and cyt b mRNAs with the exception of ATP6 (long-lived). Similarly, the analysis of NLRX1 immunoprecipitate showed more than five-fold enrichment of ND5 and cyt b mRNAs but a decrease in enrichment of COX I, COX II, ATP8 mRNAs and 16S rRNA as compared to FSATKD5. Interestingly, the analysis of FASTKD5 immunoprecipitate from cells co-transfected with both NLRX1 and FASTKD5, revealed a significant decrease in the enrichment of all FASTKD5-target RNA suggesting that NLRX1 inhibits the binding of mitochondrial transcripts to FASTKD5.

To further confirm if dynamic interaction of endogenous NLRX1 with FASTKD5 regulates its mitochondrial transcript binding, we performed RNA-IP of endogenous NLRX1

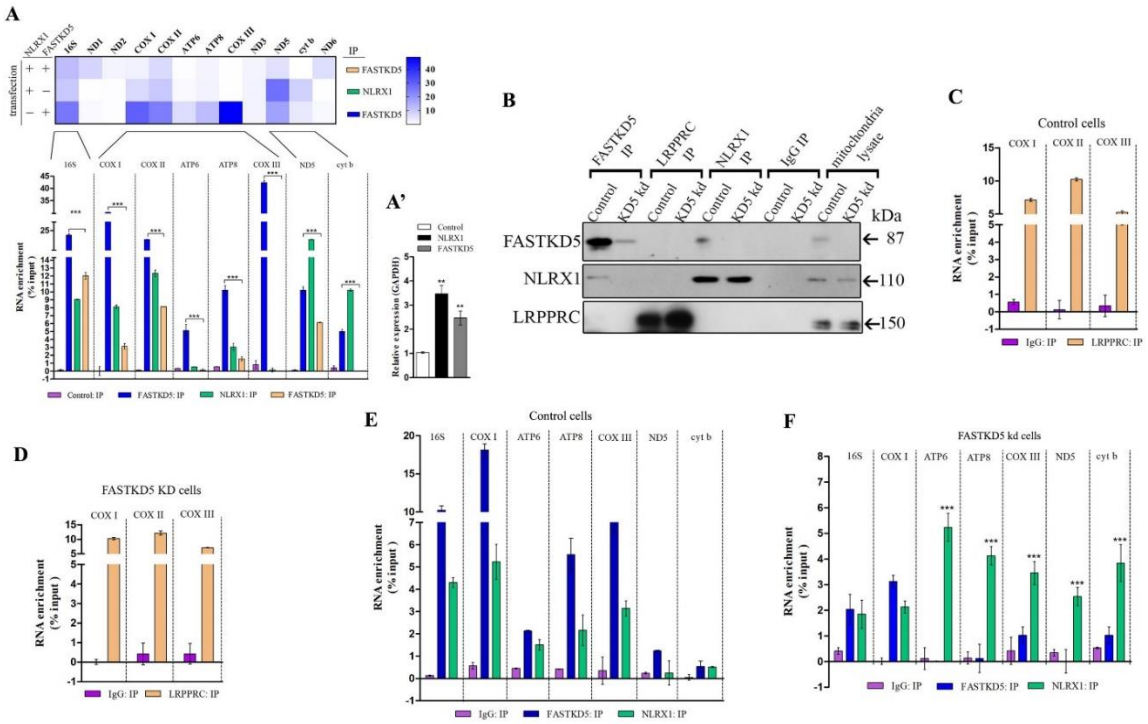

Figure 6.4: NLRX1 binds to mitochondrial RNA and regulates the processing by FASTKD5. (A) *and* ***(A')*** *HEK293 cells were transfected with NLRX1 and FASTKD5 either alone or in combination and RNA-IP was performed as described in Materials and methods. The enrichment of 16S rRNA and mt-mRNAs were quantified by qPCR and relative expression levels were represented by Heat map. Blue and white represents strong and weak enrichment respectively. Quantification of NLRX1 and FASTKD5 expression relative to nuclear control.* ***(B)*** *Mitochondrial lysates from FASTKD5 knockdown HeLa cells and control sgRNA cells were immunoprecipitated for endogenous FASTKD5, NLRX1 and LRPPRC and their pull down and input levels in IP, IgG control and mitochondrial lysate, were determined by western blotting using indicated antibody.* ***(C)*** *and* ***(D)*** *Enrichment of bound RNA by LRPPRC vs IgG from control sgRNA and FASTKD5 knockdown HeLa cells was performed by RNA-IP as described in Materials and methods.* ***(E)*** *and* ***(F)*** *Analysis of immunoprecipitated proteins in Fig. B from control sgRNA and FASTKD5 knockdown cells for bound RNA was performed as described in Materials and methods. The enrichment of mitochondrial transcripts was quantified by qPCR. Data are shown as mean ± SD (n = 3). Asterisk (*) denotes significant differences with $p < 0.05$.*

and FASTKD5 from mitochondria fraction of control and FASTKD5-KD HeLa cells. As a positive control, we immunoprecipitated LRPPRC alongside NLRX1 and FASTKD5. The analysis of protein fractions after immunoprecipitation confirmed the knockdown of FASTKD5 (Fig. 6.4B). The pulldown of both NLRX1 and FASTKD5 was detected in

respective immunoprecipitates of control cells while none of them co-immunoprecipitated with LRPPRC as observed in Fig. 6.2A. As reported previously, the analysis of RNA enrichment from LRPPRC immunoprecipitate indicated a strong association with COX I, COX II and COX III mRNAs and depletion of FASTKD5 levels did not altered this association, further validating LRPPRC as mtRNA-binding protein (Chujo et al., 2012) (Fig. 6.4C and D). In agreement with the enrichment of mitochondrial RNAs by ectopically expressed FASTKD5, the analysis of endogenous FASTKD5 immunoprecipitate from control cells showed a similar enrichment of 16S rRNA, COX I, ATP8, ATP6 and COX III mRNAs, except ND5 and cyt b. This enrichment was significantly decreased in FASTKD5 knockdown cells (Fig. 6.4E and F). The analysis of endogenous NLRX1 immunoprecipitate revealed a weak but significant enrichment of all five target RNAs of FASTKD5 in control cells which further led to the significant increase in binding of ATP8, ATP6, COX III, ND5 and cyt b mRNAs in FASTKD5 knockdown cells. These results confirmed that NLRX1 predominantly associates with ATP8/6+COX III and ND5+cyt b transcripts with high affinity and negatively regulates FASTKD5-mediated processing.

6.5 The LRR domain of NLRX1 is required for its association with FASTKD5 and mitochondrial RNA binding

The conserved LRR domain of NOD family receptor proteins has been reported to sense and bind to intracellular ligands. The LRR domain at the C-terminal-end of NLRX1 has been reported to bind single or double-stranded RNA *ex situ* (Hong et al., 2012). Therefore, to validate our hypothesis, we generated a NLRX1-truncation mutant lacking LRR domain (NLRX1-ΔLRR-Flag) and analyzed its subcellular localization by immunoblotting in HEK293 cells. We detected the bands of 110 kDa and 75 kDa corresponding to NLRX1 and NLRX1-ΔLRR exclusively in the mitochondrial fraction (Fig. 6.5A and B). Finally, we immunoprecipitated NLRX1 and NLRX1-ΔLRR from the mitochondrial lysates of HEK293 cells and analyzed the enrichment of mitochondrial RNA from respective immunoprepitates (Fig. 6.5C). As a control, we immunoprecipitated FASTKD5 alongside NLRX1 and NLRX1-ΔLRR. The analysis of protein fractions after immunoprecipitation

confirmed the pulldown of both NLRX1 and NLRX1-ΔLRR in the IP fraction. Importantly, FASTKD5 coprecipitated only with full length NLRX1, suggesting that FASTKD5 interacts with NLRX1 through the LRR domain.

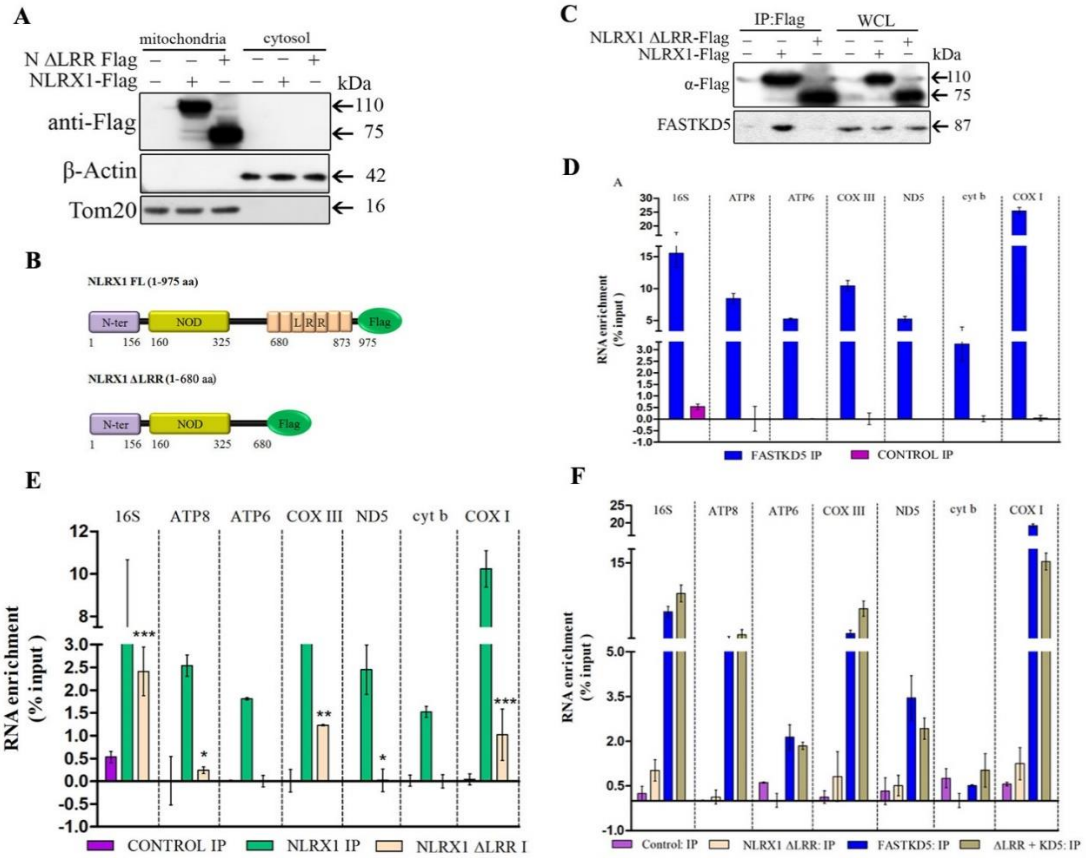

Figure 6.5: NLRX1 interacts with FASTKD5 and binds to mitochondrial RNA through LRR domain. ***(A)*** *and* ***(B)*** *HEK293 cells were transfected with NLRX1-Flag and NLRX1-ΔLRR-Flag constructs and their subcellular localization was determined by cellular fractionation and western blotting as described in Materials and methods using indicated antibodies. Schematic representation of the LRR domain deleted construct of C-terminal Flag tag-NLRX1 generated for further study.* ***(C)*** *Co-immunoprecipitation of NLRX1, NLRX1-ΔLRR by anti-Flag beads and FASTKD5 by anti-HA beads were performed from mitochondrial lysates of HEK293 cells lysate transfected with these constructs and analyzed by western blotting using indicated antibodies.* ***(D)*** *Enrichment of mitochondrial RNA by FASTKD5 vs IgG control from HEK293 cells was performed by RNA-IP and further quantified as described in Materials and methods.* ***(E)*** *and* ***(F)*** *IP Beads from (C) were further analyzed by RNA-IP as described in Materials and methods. The enrichment of mitochondrial RNA was quantified using qPCR. Data are shown as mean ± SD, (n = 3). Asterisk (*) denotes significant differences with $p < 0.05$.*

The quantification of bound RNA from NLRX1 immunoprecipitate revealed a similar enrichment of 16S rRNA, COX I, ATP8, ATP6, COX III, ND5 and cyt b mRNAs indistinguishable from the enrichment by FASTKD5 immunoprecipitate (Fig. 6.5D and E). In contrast, deletion of LRR domain led to a significant decrease in enrichment of all mRNAs of heavy strand transcripts from NLRX1-ΔLRR immunoprecipitates. These results suggested that the binding of NLRX1 to mtRNA is mediated through the LRR domain. To further investigate if LRR domain of NLRX1 essential for its interaction with FASTKD5 could also affect FASTKD5-RNA binding, we immunoprecipitated FASTKD5 from cells with or without co-expressed NLRX1-ΔLRR and analyzed the enrichment of target transcripts (Fig. 6.5F). We did not observe any significant decrease in enrichment of the heavy strand transcripts by FASTKD5 immunoprecipitates from cells transfected with FASTKD5 alone or in combination with NLRX1 ΔLRR in contrast to Fig. 6.4A where co-expression of full length NLRX1 significantly decreases the enrichment by FASTKD5. These results suggested that NLRX1 recognizes and binds to the non-junctional heavy strand transcripts specifically ND5 and cyt b mRNAs through LRR domain and negatively regulates the levels of 16S rRNA, COX I, ATP8, ATP6 and COX III mRNAs via its interaction with FASTKD5.

6.6 NLRX1 regulates the translation of mtDNA-encoded proteins and assembly of OxPhos supercomplexes

To understand the functional significance of NLRX1-regulated control of mt-RNA processing we analyzed the organization and enzyme activity of MRC complexes. Using Click azide/alkyne chemistry, we monitored the alterations in the levels of mtDNA-encoded nascent protein subunits by immunoblotting in NLRX1-expressing MCF-7 cells. A global decline in the levels of mitochondrial translation products was detected in NLRX1-transfected cells which is in agreement with the decreased levels of mature mitochondrial RNAs as observed above (Fig. 6.6A). However, this decrease was not uniform. The levels of non-canonical ATP8+COX III and ND5+cyt b precursor products: ND5, cyt b and COXIII subunits were significantly decreased (Fig. 6.6A'). Similarly, levels of ND1, ND3 and COX1 subunits were decreased, whereas levels of the remaining protein

subunits were not significantly altered. Conversely, knockdown of NLRX1 in HeLa cells increased the levels of mtDNA-encoded proteins subunits (Fig. 6.6B).

The protein subunits encoded by mtDNA are essential for the assembly and function of individual MRCs, as well as their supercomplexes. The individual CI, CIII, and CIV complexes assemble to form intermediate supramolecular assemblies known as supercomplexes (SCs) or respirasomes (Acin-Perez et al., 2008). We analyzed the levels and organization of supercomplexes in NLRX1-transfected MCF-7 cells by immunoblotting and probed for NDUFS2, a nuclear-encoded protein subunit of CI (Fig. 6.6C). The level of SCs composed of CI+CIII$_2$+CIV$_n$ and CIII$_2$+CIV decreased in the NLRX1-transfected cells as compared to vector control. The levels of individual CI and dimeric CIII and CIV also decreased, whereas levels of monomeric CIV remained unaltered.

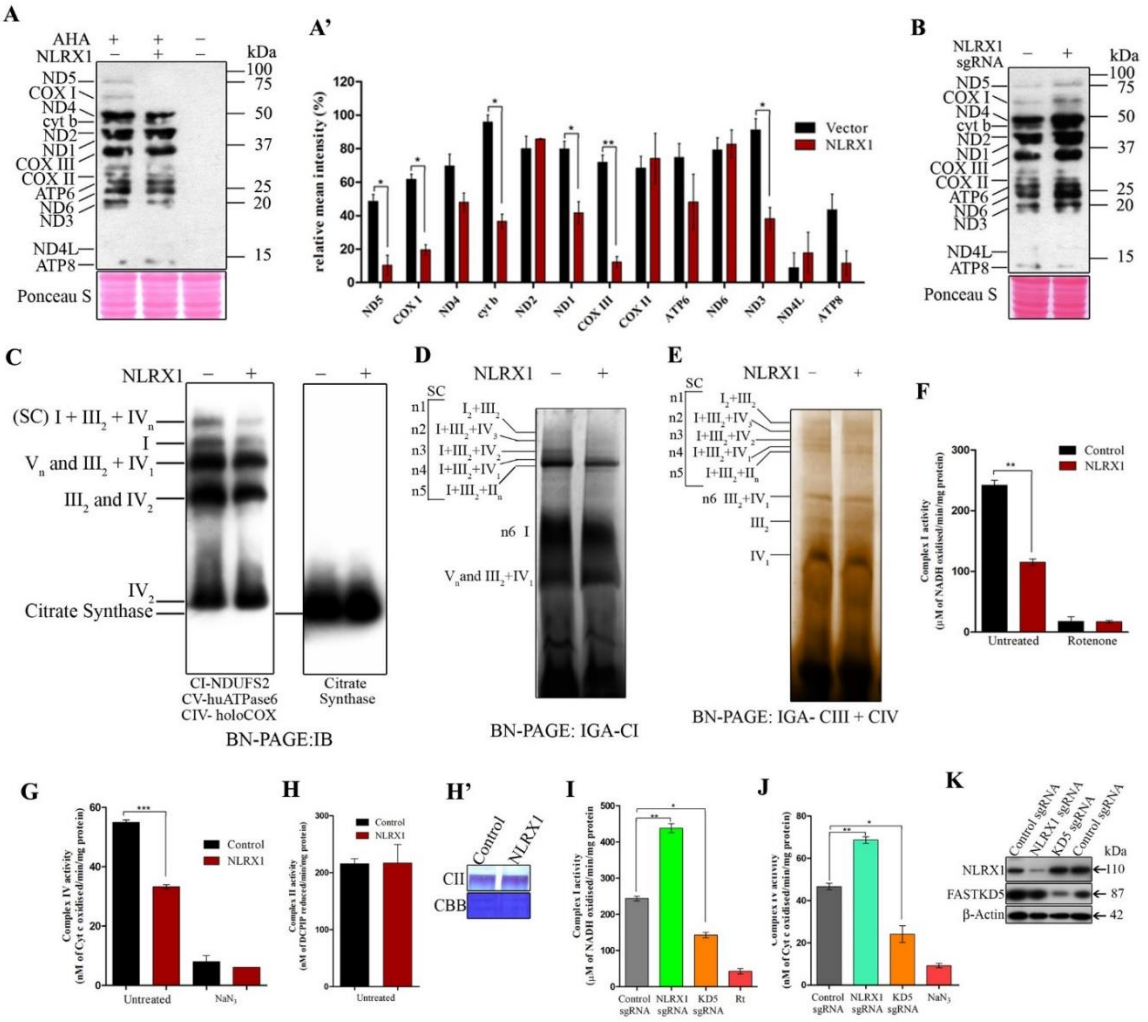

Figure 6.6: NLRX1 expression decreases the levels of mtDNA-encoded protein subunits, OxPhos activity and assembly. (A) and (A') *MCF-7 cells were transfected with control vector and NLRX1 and the levels of nascent mitochondrial protein subunits were determined after AHA (Methionine homologue) incorporation followed by analysis using Click iT® AHA chemistry and immunoblotting with anti-biotin antibody. Normal methionine incorporated (without AHA) cells were used as positive control. Quantification of band intensity of (A) detected by western blotting was performed by densitometric analysis using ImageJ v1.45 (NIH, MD, USA) software.* ***(B)*** *HeLa cells were transfected with control sgRNA and NLRX1 sgRNA and were labeled and processed as described in (A). PVDF membranes were stained with Ponceau S to assess equal protein loading.* ***(C)*** *MCF-7 cells were transfected with control vector and NLRX1 and levels of respirasomes (I + III_2 + IV_n) and supercomplex of CIII and CIV as well as individual levels were detected by BN-PAGE followed by immunoblotting with indicated antibodies. Citrate Synthase was used as loading control.* ***(D)*** *Assembly and activity of CI containing supercomplexes and individual CI were determined by BN-PAGE followed by in-gel activity staining specific for CI.* ***(E)*** *Assembly and activity of CIII and CIV containing supercomplexes and individual CIII and CIV were determined by BN-PAGE followed by in-gel activity staining specific for CIII+CIV.* ***(F)*** *and* ***(G)*** *MCF-7 cells were transfected with vector and NLRX1 and complex-I and complex-IV activity was measured using spectrophotometer.* ***(H)*** *and* ***(H')*** *MCF-7 cells were transfected with vector and NLRX1 and complex-II activity was measured spectrophotometric assay and BN-PAGE followed by in-gel activity as described in Materials and method.* ***(I)*** *and* ***(J)*** *Hela cells were transfected with control sgRNA, NLRX1 sgRNA or FASTKD5 sgRNA and enzyme activity of CI and CIV were quantified using spectrophotometer.* ***(K)*** *Confirmation of the NLRX1 and FASTKD5 knockdown in HeLa cells was assessed by western blotting using indicated antibodies. Data are shown as mean ± SEM ($n \geq 3$). Asterisk (*) denotes significant differences with $p < 0.05$.*

We further analyzed the functional activity of supercomplexes by BN-PAGE and in-gel activity staining for CI and CIII+CIV. The in-gel activity of CI in control MCF-7 cells revealed NADH dehydrogenase activity in all bands, corresponding to supercomplexes (bands n1 to n5), and to the individual CI (band n6). The ectopic expression of NLRX1 decreased the activity of free CI and the supercomplexes (Fig. 6.6D). Similarly, the in-gel staining for CIII+CIV was present in all bands of SCs (n1 to n5 and n6) and the maximum signal was detected for the monomeric CIV in control MCF-7 cells (Fig. 6.6E). In contrast, the activity of SCs (band n1 to n5), CIII dimers and monomeric CIV decreased in NLRX1-expressing cells. Similarly, the quantification of enzyme kinetic activity of individual CI and CIV of NLRX1-expressing MCF-7 cells showed as decrease in catalytic activity (Fig. 6.6F and G). However, the ectopic expression of NLRX1 did not affected the

enzyme activity of CII (Fig. 6.6H and H'). Conversely, CRISPR-Cas9-mediated knockdown of NLRX1 in HeLa cells significantly increased the enzyme activity of CI and CIV while knockdown of FASTKD5, as previously reported, decreased this activity (Fig. 6.6I, J and K). Collectively, these data demonstrated that NLRX1 modulates the organization and activity of OxPhos complexes.

6.7 NLRX1 regulates OxPhos-dependent cell proliferation of cancer cells.

To reveal the patho-physiological implications of NLRX1-regulated function in mitochondria, we monitored the growth rates of NLRX1-transfected T47D and MCF-7 breast cancer cells and HEK293 cells in a medium containing alternative primary carbon sources, namely glucose or galactose. In high-glucose medium, the growth rate of the NLRX1-transfected T47D, MCF-7and HEK293 cells did not altered significantly up to day five (Fig. 6.7A, B and C). Supposedly, the bioenergetic limitations due to the impaired OxPhos in NLRX1-expressing cells could be compensated by an increased glycolysis in the high glucose medium. This is in agreement with the previous observation by Soares *et al* reporting that NLRX1 increases cellular proliferation by activating the glycolytic metabolism (Soares et al., 2014).

In galactose-containing medium, the growth rate of control cells was lower, as compared to the high glucose medium (Fig. 6.7D, E and F). Apparently, the NADH consuming and bioenergetically less efficient conversion of galactose to glucose-1-phosphate is unable to provide the increased energy demands of proliferating cells causing an increased dependence on mitochondrial respiration (Robinson et al., 1992). In agreement, we observed an overall decreased growth rate of NLRX1-expressing T47D, MCF-7and HEK293 cells in the galactose medium. The proliferation rate of cells remain unchanged during the initial 48 h, thereafter the rate gradually declined and stopped proliferating after day 5 suggesting a compromised OxPhos activity.

We also monitored the functional role of NLRX1 in regulating survival and proliferation of MCF-7 and T47D cells in both glucose or galactose containing medium. The proliferation rate of vector-transfected control cells showed no change in both medium, but NLRX1-transfected cells exhibited a retarded proliferation in galactose medium (Fig.

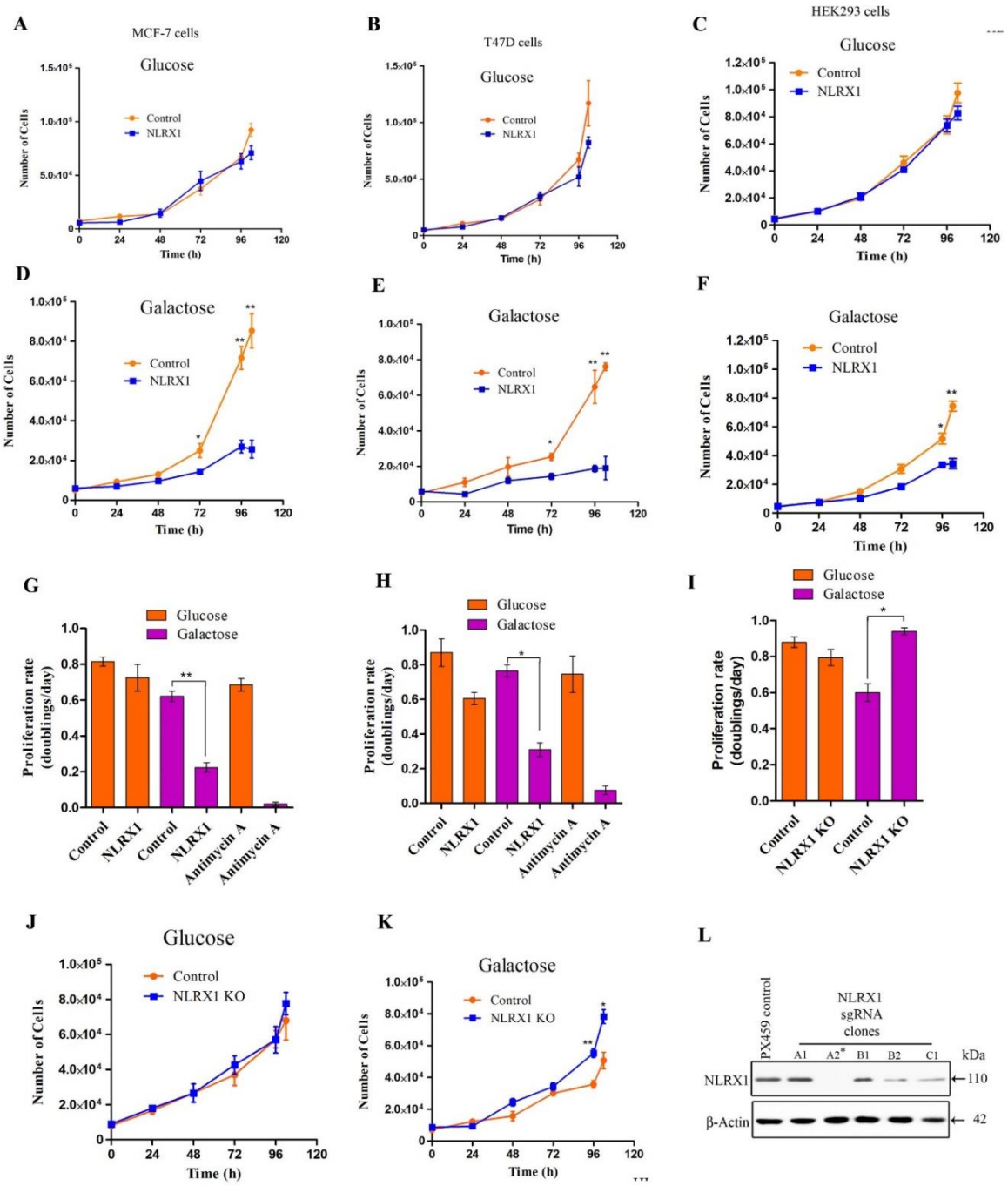

Figure 6.7: Ectopic expression of NLRX1 decreases the proliferation of OxPhos-deficient cells. (A), (B), (C), (D), (E) and (F) *MCF-7, T47D and HEK293 cells were transfected with vector and NLRX1. After transfection, cells were seeded in glucose/galactose-containing medium with or without antimycin A (100 nM). Growth curves were determined by cell count normalized to cell number at t = 0 when media conditions were applied, were assessed for five consecutive days and used to calculate proliferation rate.* ***(G)*** *and* ***(H)*** *Proliferation rates of the cells in respective medium were determined as described in Materials and methods.****(I)****,* ***(J)*** *and* ***(K)*** *Control and NLRX1 KO HEK293 cells were seeded in glucose/galactose containing*

medium and growth curves were obtained and proliferation rate calculated as described in Materials and methods. ***(L)*** *HEK293 cell were transfected with PX459 control and NLRX1 sgRNA vector. Stable cell clones were selected and cultured as described in Materials and method. The clone A2 marked with an asterisk is referred to as NLRX1 knockout cell line and was used for cell proliferation assay*

6.7G and H). Furthermore, a severe decrease in proliferation rate of cells growing in the galactose medium was observed in the presence of antimycin A, the CIII inhibitor, but not in high glucose medium. Therefore, the NLRX1-expressing cells with dysfunctional OxPhos function are unable to proliferate in galactose medium. Conversely, the CRISPR-Cas9 mediated knockout of NLRX1 significantly increased the proliferation rate of HEK293 cells in the galactose medium (Fig. 6.7I, J, K and L). These results confirmed that NLRX1-expression impairs mitochondrial respiratory function causing an increased dependence on glycolysis of cell survival and proliferation.

6.8 Discussion

Investigating the precise submitochondrial localization of NLRX1 and its mechanism of regulating mitochondrial function is not only critical for understanding the metabolic re-programming during innate immune activation but also for maintaining cellular bioenergetic capacity during metabolic adaptation in cancer cells. Here, we demonstrated that association of NLRX1 and FASTKD5 negatively regulates mitochondrial RNA processing and metabolic adaptation of cancer cells.

In the present study, we systematically characterized the sub-mitochondrial localization of NLRX1. We show that NLRX1 is a mitochondrial protein and specifically localizes to mitochondrial matrix. This conclusion is in agreement with Arnoult *et al*. reporting that NLRX1 is targeted to mitochondrial matrix (Arnoult et al., 2009). The live-cell imaging data further confirmed the colocalization of NLRX1 with mitochondrial matrix-targeted proteins in different cell lines. The low levels of cytoplasmic NLRX1 detected during sub-cellular fractionation potentially explains the discrepancy in the localization and function of NLRX1 reported by other groups (Rebsamen et al., 2011; Soares et al., 2013). The cytoplasmic pool of NLRX1 may interact and initiate the degradation of MAVS at the mito-

chondrial outer membrane, thereby negatively regulating type-I IFN and NF-κB activation during antiviral response (Qin et al., 2017). Additional studies are needed to understand if the mitochondrial localization of NLRX1 is important for innate immune signaling, or the cytoplasmic NLRX1 is alone sufficient.

The potential ligands and effector functions of NLRX1 within mitochondria is still unknown. mtDNA-encoded mRNAs are maintained at distinct steady-state levels which vary in their abundance across different tissues to ensure proper stoichiometry of OxPhos complex (Benard et al., 2006; Mercer et al., 2011). The mature mitochondrial mRNAs are generation through post-transcriptional processing of polycistronic mRNAs within MRGs (Pearce et al., 2017). Using co-immunoprecipitation experiments, we confirmed the interaction of NLRX1 with FASKD5 in mitochondria. Similarly, confocal and super-resolution imaging revealed the colocalization of NLRX1 and FASTKD5 with MRGs and its punctate size and distribution within mitochondria. Our results strongly indicate that NLRX1 is a novel protein component of MRGs where it dynamically interacts with FASTKD5. The analysis of mature mitochondrial transcripts revealed a significant reduction in the steady-state levels of non-canonical mt-mRNAs, such as COX I, ATP8/6, COX III, ND5, cyt b in NLRX1-expressing cells and deletion of the N-terminal addressing sequence prevented the localization of NLRX1 to mitochondria leaving causing the levels of mature mt-mRNAs unchanged. This strongly suggested that targeting of NLRX1 to mitochondrial matrix is essential for the regulation of RNA processing within MRGs. FASTKD5 is a bonafide MRG protein which is required for the processing of three non-canonical heavy-strand precursor transcripts (5’end-COX I, ATP8/6+COX III, and ND5+cyt b), as depletion of FASTKD5 resulted in an accumulation of unprocessed precursor RNAs and defective complex IV (Antonicka and Shoubridge, 2015). The ectopic expression of NLRX1 decreases the steady state levels of ATP8/6, COX III, ND5 and cyt b mRNAs thus preventing their maturation by binding directly to these transcripts as shown by RNA-IP of NLRX1. Further, the association of NLRX1 with FASTKD5 may modulate the processing and maturation of non-canonical precursor transcripts. Additionally, in the absence of FASTKD5, NLRX1 strongly binds to ATP8/6, COX III, ND5 and cyt b mRNAs and negatively regulates the maturation of these transcripts. This observation is further sup-

ported by accumulation of ATP8/6+COX III, and ND5+cyt b unprocessed heavy strand transcripts in FASTKD5-KD cells as reported earlier (Antonicka and Shoubridge, 2015).

The C-terminal LRR domain of NLRX1 (residues 629-975, cNLRX1) is stabilized by inter-subunit and inter-domain interactions to form compact hexameric architecture. A previous study demonstrated that cNLRX1 can directly bind to ssRNA analogue *ex situ* (Hong et al., 2012), although no data with live cells has been reported and its implication in cellular function is unknown. In the present study, using RNA-IP, we demonstrated the enrichment of a distinct set of mt-mRNAs by NLRX1, as compared to FASTKD5, however, C-terminal deletion showed no enrichment, suggesting that LLR domain of NLRX1 is essential for binding to RNA as well as its interaction with FASTKD5. Thus, NLRX1 may directly bind to mitochondrial transcripts and regulate its processing and maturation, as well as indirectly by sequestering FASTKD5.

The mature mitochondrial mRNAs are translated to 13 essential protein subunits of mitochondrial respiratory chain complexes constituting the OxPhos system. Although, a global decline in the levels of mtDNA-encoded protein subunits was detected in NLRX1-expressing cells, we observed a selective decrease in the mtDNA-encoded CI (ND1, ND3 and ND5), CIII (cyt b) and CIV (COX I and COX III) protein subunits. The ectopic expression of NLRX1 also decreased levels of mature 16SrRNA suggesting that the biogenesis of mitochondrial ribosome may be affected. The sequestration or binding of NLRX1 to FASTKD5 may negatively regulate the assembly of mito-ribosomes and thus the translation of mt-mRNA. A previous report demonstrating the role of FASTKD5 in mitochondrial ribosome biogenesis and now its association with NLRX1 further supports this hypothesis (Antonicka and Shoubridge, 2015). Similarly, the interaction of NLRX1 with TUFM (Tu translation elongation factor, mitochondrial) and its role in antiviral response has been previously reported, however its implication in regulation of mitochondrial translation has not been investigated (Lei et al., 2012). Our findings here suggest that NLRX1 may be important for RNA processing and mito-ribosome biogenesis and translation.

The assembly and activity of individual MRC complexes are mediated through mtDNA-encoded protein subunits. The overall decrease in synthesis of mtDNA-encoded protein subunits resulted in a combined defect in assembly of supercomplexes containing CI, CIII

and CIV including individual complexes. An impaired assembly of respirasomes induces oxidative stress by an excessive generation of ROS (Lopez-Fabuel et al., 2016). We and others have previously reported the increased generation of ROS in response to NLRX1 overexpression (Singh et al., 2015; Tattoli et al., 2008). Here, we found that NLRX1 selectively decreased the enzyme activity of CIV in supercomplex, or in its uncomplexed state. A defective OxPhos assembly compromises mitochondrial respiration, which is supported by our observation that NLRX1 expressing cells proliferate poorly in the medium containing galactose instead of glucose.

In conclusion, our study establishes a critical role of NLRX1 in regulating the post-transcriptional processing of mitochondrial precursor mRNAs to modulate the steady state levels of mature mitochondrial RNAs, thus, controlling the activity and organization of OxPhos complexes. We and others have reported that NLRX1 may act as a potential tumor suppressor in breast and colorectal cancer (Lei and Maloy, 2016; Singh et al., 2015). NLRX1-mediated regulation of mitochondrial gene expression may play an important role in metabolic reprogramming of tumor cells. However, this observation needs to be further studied and validated in different experimental models of cancer.